Vapor Dynamics of Heat Pipe Start-Up

F. Issacci
Assoc. Mem. ASME

I. Catton
Fellow ASME

N. M. Ghoniem
Professor.

Mechanical, Aerospace, and Nuclear Engineering, University of California—Los Angeles, Los Angeles, CA 90024-1509

Vapor dynamics of heat pipes during the start-up phase of operation is analyzed. The vapor flow is modeled by a two-dimensional, compressible viscous flow in an enclosure with inflow and outflow boundary conditions. For high-input heat fluxes, a compression wave is created in the evaporator early in the operation. A nonlinear filtering technique, along with the centered difference scheme, is used to capture the shocklike wave and overcome the cell Reynolds number problem. Multiple wave reflections are observed in the evaporation and adiabatic regions. These wave reflections cause a significant increase in the local pressure and flow circulations, which grow with time. It is shown that the maximum and maximum-averaged pressure drops oscillate periodically because of the wave reflections. Although the pressure drops converge to a constant value at steady state, they are significantly higher than their steady-state value at the initiation of the process. The time for the vapor core to reach a steady-state condition was found to be on the order of seconds.

Introduction

The behavior of vapor flow during the start-up phase of heat pipe operation has been analyzed in order to examine the flow patterns for low and high-input heat fluxes. Here, start-up is the process through which the heat pipe starts its operation from a static condition and arrives at steady-state operation. The response of the vapor flow may be an important design issue in dynamic thermal systems where a heat pipe is used to transfer heat following sudden increases in the heat load. The importance of the transient phase, of course, depends on many factors not considered here.

During a start-up, the working fluid of a heat pipe may initially be very cold or frozen in the wick. Here, the liquid is assumed to be very cold and the vapor, which is thermodynamically in equilibrium with the liquid, is at very low pressure. The vapor core response to a sudden-input heat flux or a sudden change in the condenser temperature is the primary focus of this work.

The vapor flow in heat pipes is a complicated problem because of the nonlinear nature of the describing equations and because of the inflow and outflow boundaries in the evaporator and condenser. Different approaches have been used to simplify the problem. In most previous work, the vapor flow is analyzed under steady-state conditions as a one-dimensional (1D) flow (e.g., Edwards and Marcus, 1971) and a 2D flow (Tien and Rohani, 1974; Faghri,1986; Faghri et al., 1989; Peterson and Tien, 1987). In studies of the dynamic behavior of heat pipes, the vapor flow is modeled either as a quasi-steady flow (Jang et al., 1989) or as a 1D transient vapor flow along with friction coefficients approximated from a steady-state 2D model (Bowman, 1987). It has been shown by steady-state 2D analysis that the 1D vapor-flow model is not able accurately to predict the axial heat and mass transfer and pressure drop (Bankston and Smith, 1973). Furthermore, 2D steady-state studies indicate that flow reversal takes place in the condensation section under high heat flux (Issacci et al., 1989). It is, therefore, important to establish the conditions for this mode during transient operations.

In a theoretical study using a 1D transient model, Bystrov and Goncharov (1983) showed that the time steps in the numerical calculations that are necessary to satisfy stability requirements are small (order of 10^{-7} s). The numerical scheme used in this work is fully implicit, which allows larger time steps (up to order of 10^{-2} s). The vapor dynamics of heat pipes was also studied by Issacci et al. (1989) using a 2D transient model with the SIMPLER method (Patankar, 1980). The primary advantage of SIMPLER is the staggered grid, which makes the numerical scheme stable and, consequently, the computational time low. Although this method yielded interesting results, the resulting computational code was limited to low-compressibility flows. However, in the start-up mode of a heat pipe, there are regions of high as well as low compressibility. Existing numerical codes for highly compressible flows, on the other hand, are only able to handle steady-state conditions because of their small allowable time steps and, furthermore, they are not stable for low-Mach-number problems.

Several theoretical studies have recently been carried out to model heat pipes at start-up from the frozen state (Bowman et al., 1990; Chow and Zhong, 1990; Hall and Doster, 1988, 1990; Jang et al., 1989; Rao et al., 1990). In these different approaches, the vapor core has been modeled as a 1D quasi-steady or 1D unsteady state flow.

As can be seen, the past 2D studies were limited to incompressible flows and compressible flow studies were limited to 1D. At UCLA, the study of dynamic behavior of heat pipes began by analyzing the liquid and vapor phases separately (Roche, 1988; Issacci et al., 1988). The objective was to develop very detailed computer codes for each phase and then to combine them in a comprehensive code. Roche (1988) developed a numerical code for the liquid phase in the start-up mode with the vapor phase assumed to be at a constant temperature and pressure. He used a kinetic theory approach to model the phase change at the liquid-vapor interface.

The objective of this work is to investigate thoroughly the dynamic behavior of the vapor flow in heat pipes during the start-up phase of its operation. Efforts have been directed toward understanding of the vapor flow patterns under very low pressure and high input heat flux conditions. In heat pipes under the transient mode of operations, the vapor flow is the most complicated process. A simple model of this phase is, however, needed for a fast computer code. A simple and accurate model would only be achievable if the complete vapor process was understood in detail. The studies carried out in this paper are aimed at this understanding.

The fully compressible describing equations of the vapor flow are numerically solved using a transient 2D model. The

Contributed by the Heat Transfer Division for publication in the JOURNAL OF HEAT TRANSFER. Manuscript received by the Heat Transfer Division March 27, 1990; revision received March 8, 1991. Keywords: Heat Pipes and Thermosyphons, Numerical Methods, Transient and Unsteady Heat Transfer.

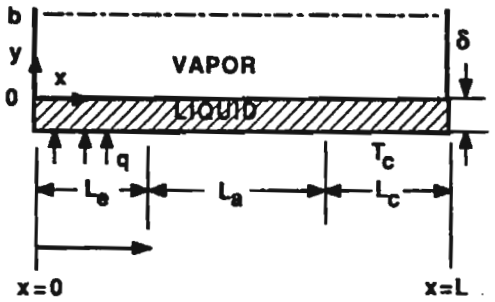

Fig. 1 Vapor flow model in a heat pipe

numerical scheme is fully implicit using a staggered grid, and it is stable for all Mach numbers between zero and one, a suitable range for the start-up transient mode. The effect of wall and wick structure is not included here. As mentioned above, the main concern is the detailed study of vapor phase to be coupled later to other phases in the heat pipe. The transient characteristics of the wall and wick structure affect the vapor flow patterns. However, the results of the vapor phase study will help significantly in the complete model of heat pipes.

2 Describing Equations

Vapor flow in the heat pipe core is modeled as channel flow, as is shown in Fig. 1. The bottom boundary of the channel is a thin porous medium, which contains the liquid. The input heat flux to the evaporator and the temperature of the outer surface of the condenser are specified. The planar side walls are assumed adiabatic.

The equations describing the vapor flow are the continuity, momentum, and energy equations, which are time dependent, viscous, and compressible. An equation of state (EOS) is used to relate pressure, density, and temperature within the vapor core. These equations in Cartesian coordinates (x, y) are

Continuity

$$\frac{\partial \rho}{\partial t} + \frac{\partial (\rho u)}{\partial x} + \frac{\partial (\rho v)}{\partial y} = 0 \tag{1}$$

x Momentum

$$\frac{\partial (\rho u)}{\partial t} + \frac{\partial (\rho u u)}{\partial x} + \frac{\partial (\rho u v)}{\partial y} = -\frac{\partial p}{\partial x} + \frac{\partial}{\partial x}\left(\mu \frac{\partial u}{\partial x}\right) + \frac{\partial}{\partial y}\left(\mu \frac{\partial u}{\partial y}\right) + \left[\frac{\partial}{\partial x}\left(\mu \frac{\partial u}{\partial x}\right) + \frac{\partial}{\partial y}\left(\mu \frac{\partial v}{\partial x}\right) - \frac{2}{3}\frac{\partial}{\partial x}\left(\mu \frac{\partial u}{\partial x} + \mu \frac{\partial v}{\partial y}\right)\right] \tag{2}$$

y Momentum

$$\frac{\partial (\rho v)}{\partial t} + \frac{\partial (\rho u v)}{\partial x} + \frac{\partial (\rho v v)}{\partial y} = -\frac{\partial p}{\partial y} + \frac{\partial}{\partial x}\left(\mu \frac{\partial v}{\partial x}\right) + \frac{\partial}{\partial y}\left(\mu \frac{\partial v}{\partial y}\right) + \left[\frac{\partial}{\partial x}\left(\mu \frac{\partial u}{\partial y}\right) + \frac{\partial}{\partial y}\left(\mu \frac{\partial v}{\partial y}\right) - \frac{2}{3}\frac{\partial}{\partial y}\left(\mu \frac{\partial u}{\partial x} + \mu \frac{\partial v}{\partial y}\right)\right] \tag{3}$$

Energy

$$C_p\left[\frac{\partial (\rho T)}{\partial t} + \frac{\partial (\rho u T)}{\partial x} + \frac{\partial (\rho v T)}{\partial y}\right] = \frac{\partial p}{\partial t} + u\frac{\partial p}{\partial x} + v\frac{\partial p}{\partial y} + \frac{\partial}{\partial x}\left(k\frac{\partial T}{\partial x}\right) + \frac{\partial}{\partial y}\left(k\frac{\partial T}{\partial y}\right) + \mu\left[2\left(\frac{\partial u}{\partial x}\right)^2 + 2\left(\frac{\partial v}{\partial y}\right)^2 + \left(\frac{\partial u}{\partial y} + \frac{\partial v}{\partial x}\right)^2\right] \tag{4}$$

EOS

$$p = \rho R T \tag{5}$$

Here, the vapor flow is assumed to be a perfect gas; however, Eq. (5) can be replaced by a more realistic EOS with no major difficulty in calculations.

2.1 Initial and Boundary Conditions. The working liquid is assumed initially to be at a low temperature (close to the freezing point). Further, there is no input heat and the stagnant vapor is in thermodynamic equilibrium with the liquid. The boundaries of the vapor core are shown in Fig. 1. A no-slip and impermeable condition for the velocity and an adiabatic condition for the temperature are assumed on the side walls, i.e., at $x = 0$ and $x = L$ as

$$u = 0, \quad v = 0, \quad \partial T/\partial x = 0 \tag{6}$$

On the centerline the symmetry condition implies, at $y = b$,

$$\partial u/\partial y = 0, \quad v = 0, \quad \partial T/\partial y = 0 \tag{7}$$

The boundary conditions at the liquid–vapor interface are the challenging ones. The liquid flow is assumed to be in a porous medium of thickness δ, which is much smaller than the vapor core thickness b. The axial velocity is assumed zero on this boundary, i.e., at $y = 0$,

$$u = 0 \tag{8}$$

To assign boundary conditions for the temperature and vertical velocity, the liquid–vapor interface is divided into three regions. In the evaporation zone the input flux, $\dot{q}''$, is a given parameter and the input flow is approximated at $y = 0$ and $0 < x \le L_e$ by

$$\rho v = \dot{m}'' \approx \dot{q}''/h_{fg}(T), \quad T = T_{sat}(p) \tag{9}$$

where h_{fg} is the heat of vaporization and $\dot{m}''$ is the input mass

Nomenclature

b = channel width
C_p = specific heat
h_{fg} = latent heat
k = thermal conductivity
L = heat pipe length
L_a = adiabatic section length
L_c = condenser length
L_e = evaporator length
$\dot{m}''$ = mass flux
N_x = number of grid points in x direction
N_y = number of grid points in y direction
p = pressure
$\dot{q}''$ = input heat flux
R = gas constant
Re = Reynolds number
T = temperature
t = time
u = axial velocity
v = vertical velocity
x = axial coordinate
y = vertical coordinate
δ = liquid layer thickness
Δt = time increment
λ = constant factor
μ = viscosity
ρ = density
ϕ = general dependent variable
ϕ^r = referenced value of ϕ

Subscripts

c = condenser
eff = effective
o = initial value
sat = saturation

flux. Conduction in the liquid layer is neglected. It should be noted that this boundary condition ignores the thermal characteristics of the heat pipe wall and the working fluid-wick layer. The temperature is assumed to be the saturation temperature $T_{sat}(p)$ of the liquid corresponding to the interface pressure. In the adiabatic zone, the boundary conditions at $y = 0$ and $L_e < x \leq (L_e + L_a)$ are

$$v=0, \quad \partial T/\partial y=0 \tag{10}$$

In the condensation zone the temperature T_c of the outer surface is given. T_c could well vary with time, as it is usually related to the ambient temperature by convection and/or radiation heat transfer. Here, T_c is assumed fixed, which is the equivalent to assuming very good heat transfer to the surroundings. By equating the heat of evaporation to the heat conduction in the liquid layer, the outflow from this region is approximated at $y = 0$ and $(L_e + L_a) < x \leq L$, by

$$\rho v=\dot{m}'' \approx -\frac{k_{\text{eff}}}{\delta}\left(\frac{T-T_c}{h_{fg}(T)}\right), \; T=T_{sat}(p) \tag{11}$$

where k_{eff} is the effective conductivity of the liquid layer and the temperature is assumed to be the saturation temperature corresponding to the pressure at the interface. This neglects transient conduction in the fluid layer, which may be an important contribution to the process.

3 Solution Method

The five describing Eqs. (1)–(5), with the initial and boundary conditions given by Eqs. (6)–(11), have been numerically solved for the five variables ρ, ρu, ρv, T, and p. A finite-difference method has been used with backward Euler discretization in time and centered differences in space. Dealing with a wide range of input heat fluxes, the method deals effectively with the cell Reynolds number problem as well as shock-capturing complexity. Discretization of the advective terms in this problem plays a significant role. The centered-difference scheme (CDS) is ill-behaved for grid Reynolds numbers larger than two because the coefficients of the difference equations are not necessarily positive. As a consequence, solutions to the difference equations may not be unique, resulting in nonphysical spatial oscillations. In a study of the 1D forms of the describing Eqs. (1)–(5) by Issacci et al. (1990b), standard methods such as upwinding and power law and a more recent scheme, CONDIF, were examined. It was shown that these schemes are well-behaved but that they cause oscillations and overshoot at high compressibility and, except for CONDIF, they cause numerical diffusion at low compressibility as well. The CONDIF scheme was used by Issacci et al. (1990a) in a study of the start-up transient process in heat pipes. It was shown that for input heat fluxes greater than 1 kW/m^2 in an Na-filled heat pipe, a shocklike wave is created in the evaporation region. Therefore, the CONDIF scheme was found to be unsuitable for shock capturing.

Recently developed methods for shock capturing that use field-by-field decomposition and flux limiting, e.g., Harten (1983) or Chakravarthy and Osher (1982), are able to capture a sharp discontinuity without ocsillations. However, these methods are complicated and are not numerically efficient. Different filters have also been used in shock capturing; cf. Harten and Zwas (1972).The major problem in filtering is the low accuracy and smearing of the shock front. Recently, Engquist et al., (1989) proposed a nonlinear filter to capture accurately a shock without oscillations. The algorithms for this filtering are simple to implement and are more efficient than earlier methods with comparable abilities.

A filtering technique, based on the concept introduced by Engquist et al. (1989), was used in a study of 1D compressible vapor dynamics by Issacci et al. (1990b). It was shown that CDS used with nonlinear filtering yields a second-order, stable solution in cell Reynolds problems and is able to capture a shock without oscillations. In the present work the same technique has been used to solve the 2D form of the describing equations for a compressible vapor flow.

The describing equations are nonlinear and coupled. An iterative method is used to solve Eqs. (1)–(5) for ρ, ρu, ρv, T, and p separately. The SOR method is used to solve the differenced equations. Iteration on the equations was stopped after convergence of all the variables. This iteration method required the least storage and fewest calculations.

4 Results

A computer code was written to implement the numerical procedure described above. The boundary conditions of inflow and outflow at different locations on the same boundary are nonlinear. Furthermore, the exit point of the evaporator and the entrance point to the condenser, on the bottom boundary, are mathematically singular points. The boundary conditions at these points have sharp gradients, which perturb the numerical scheme. In order to avoid this problem, the inflow and outflow mass fluxes are multiplied by the factor $\tanh \lambda(x-x_o)$. In the evaporator and the condenser, $x_o = 0$ and 2, respectively. Depending on λ, this factor makes the gradients smoother at the singular points. In practice, the vapor phase is coupled to the liquid phase in the heat pipe and the heat flux applied to the liquid phase will not produce a step-shape profile at the liquid–vapor interface.

For the results shown in this section, the working fluid is liquid sodium at, initially, $P_o = 10^3$ N/m^2 and $T_o = 800$ K. The geometry dimensions are $b = 5$ cm, $L_e = L_a = L_c = b$, and $\lambda = 5$. The results are shown in the following sections for low- and high-input heat fluxes and for the pressure drops along different sections of the heat pipe.

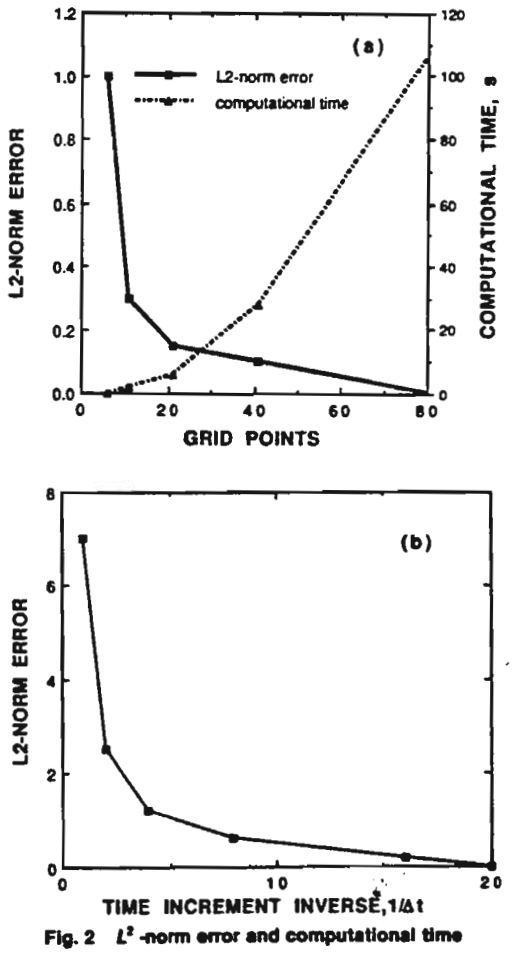

Fig. 2 L^2-norm error and computational time

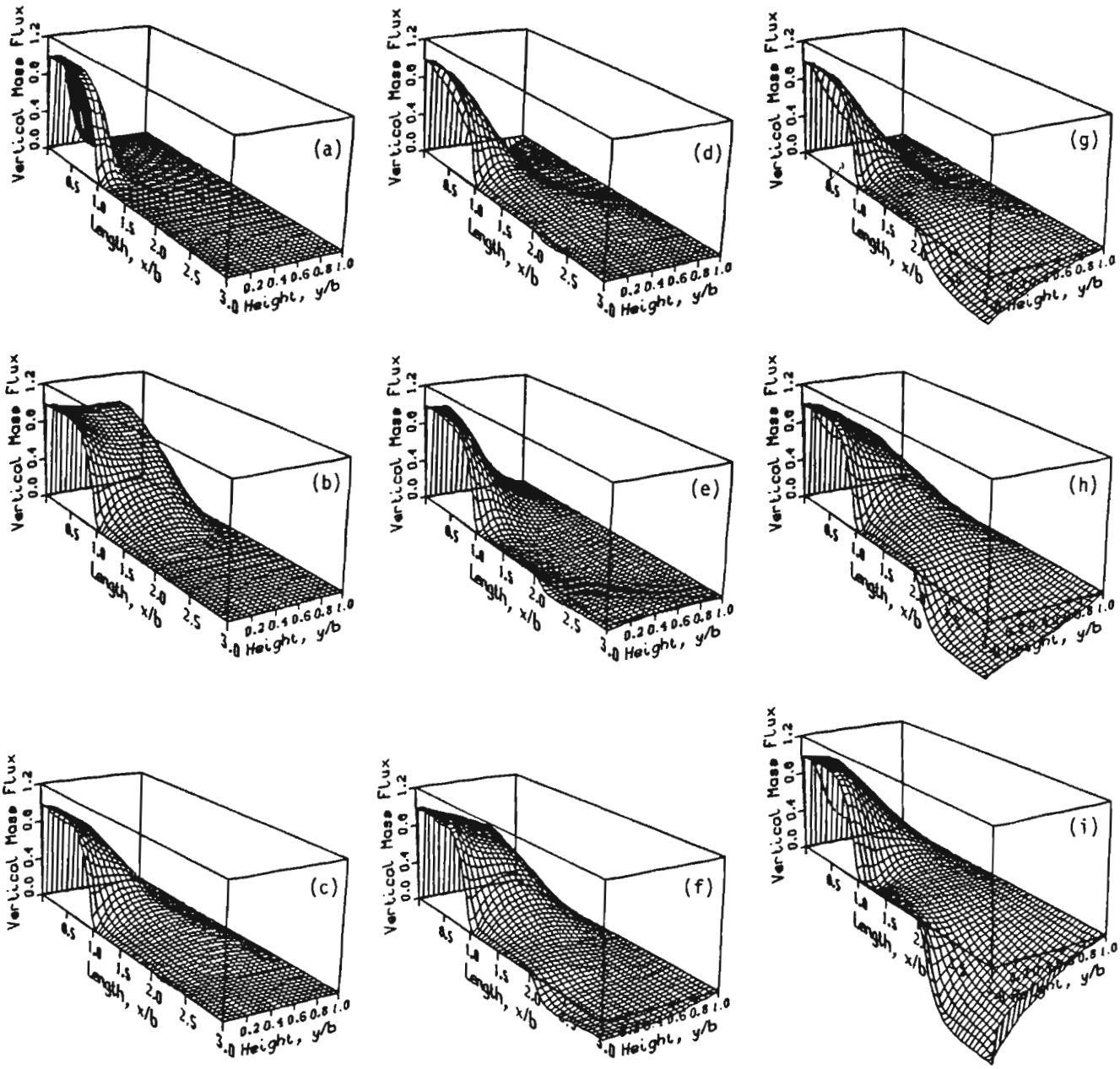

Fig. 3 Transient development of the vertical mass flux for a low-input heat flux

The calculational grid for each computation was chosen by inspection of the calculated L^2 -norm error. The L^2 -norm is defined as

$$L^2-\text{ norm} = \left[\frac{1}{N_x N_y}\sum_{i,j}\left(\frac{\phi_{i,j}-\phi^r_{i,j}}{\phi^r_{i,j}}\right)^2\right]^{1/2} \tag{12}$$

where N_x and N_y are numbers of grid points in the x and y directions, respectively. Here, ϕ is one of the dependent variables (ρ, ρu, ρv, T, or P) and ϕ^r is the calculated ϕ on the finest mesh of calculations. The results of the error analysis for a sample calculation are shown in Fig. 2. With an increase in grid points, the L^2 -norm error decreases exponentially; however, the computational time increases (Fig. 2*a*). In this sample analysis, for grid points greater than 21, the error does not decrease by much, whereas the corresponding computational time increases significantly. Therefore, for this case, the optimized grid point is 21.

The same error analysis is also carried out for time increments Δt using Eq. (12). In this case, ϕ^r is the result of calculations according to the smallest Δt. The L^2 -norm error for different time increments is shown in Fig. 2(*b*). As expected, the error decreases as Δt decreases. The sample error analysis, described above, was carried out for different input conditions in order to choose the corresponding optimized grid points and time increments.

4.1 Low-Input Heat Flux. Figure 3 shows the flow patterns in the vapor core for a low-input heat flux, $\dot{q}''_0 = 10^5$ W/m^2. The Reynolds number based on the vapor thickness is Re = 100 and the computations were done for an optimized grid of 21 × 61. The transient development of the vertical mass flux ρv at different times is shown in Fig. 3. At $t = 0$, the vapor is stagnant. Evaporation takes place as the input heat flux is applied. Since the input heat flux is relatively high, a compression wave is created (Fig. 3*a*). The vapor flow develops above the evaporator and in the adiabatic region and the wave travels above the evaporator until it hits the upper boundary (Fig. 3*b*) where the vertical mass flux is blocked, ρv

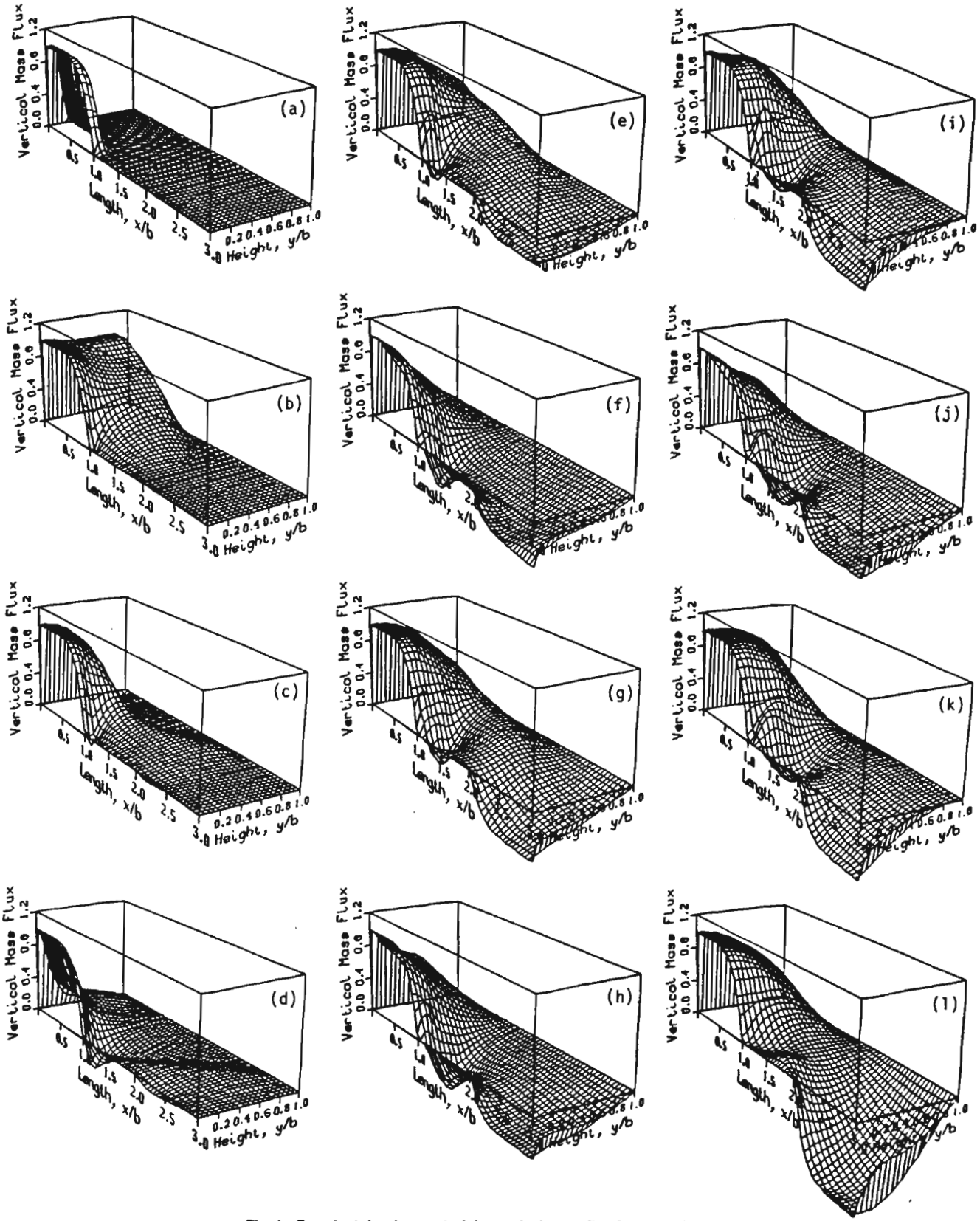

Fig. 4 Transient development of the vertical mass flux for a high-input heat flux

= 0. At this point, the vapor is compressed and the vapor pressure increases, which causes a positive vertical pressure gradient and the wave reflects back (Fig. 3*c*). The figure also shows reverse flow in the top left corner, which is caused by wave reflection. When the reflected wave reaches the lower boundary (Fig. 3*d*) and the vapor is compressed within the evaporation region, the vertical pressure gradient is reduced and the inflow mass flux tries again to fill the evaporation region (Fig. 3*e*). As the vapor fills the evaporation region (Fig. 3*f*), another wave reflection occurs and the flow reverses in

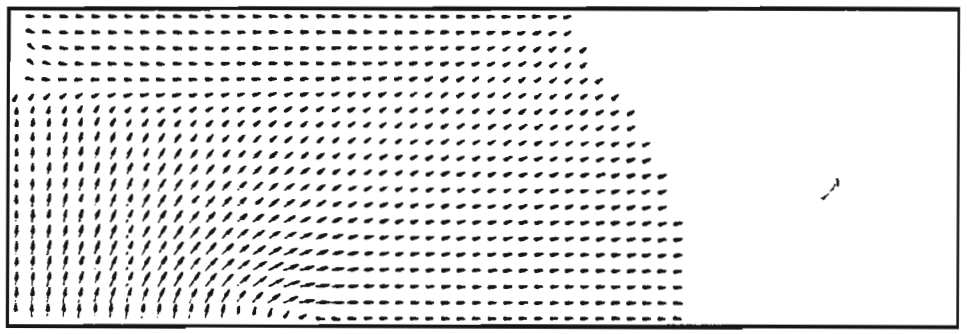

(a)

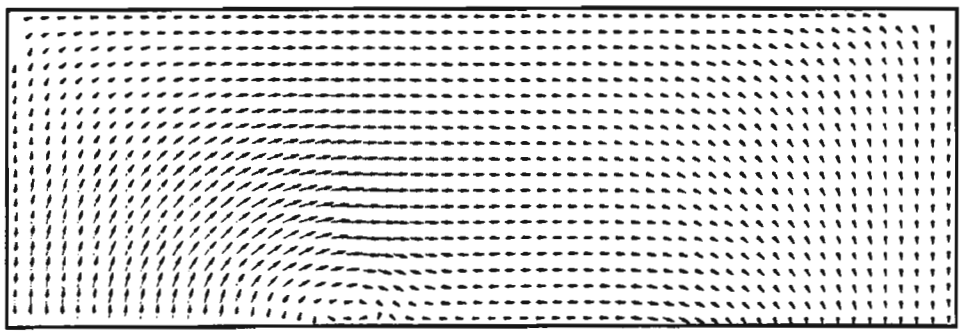

(b)

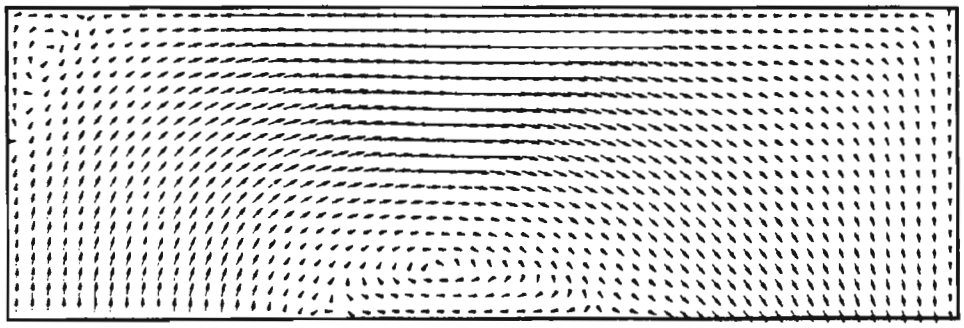

(c)

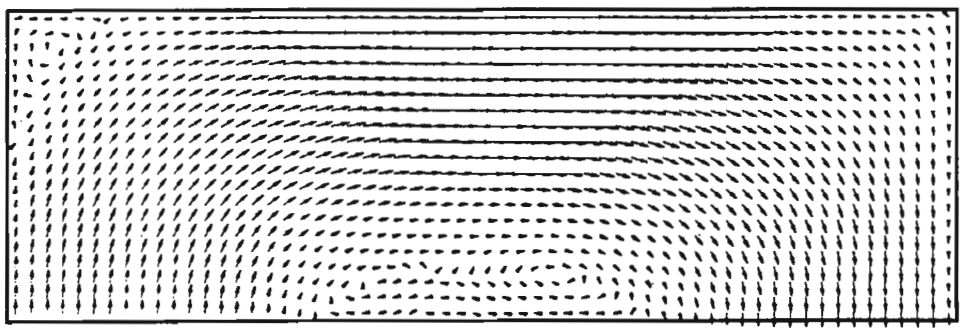

(d)

Fig. 5 Vapor flow fluids at different time levels (arrows indicate direction; tail indicates magnitude)

the top left corner (Fig. 3*g*). Comparing Figs. 3(*d*) and 3(*g*), the reverse flow after the second reflection is weaker than that in the first reflection. About eight to ten cycles of refill and reflection of mass flow are observed in the evaporation region before the process becomes steady (Fig. 3*i*). At each cycle the reverse flow is weaker and after four cycles there is no reverse flow. The vertical gradient in the mass flux ρv also decreases with each cycle.

The transient flow pattern in the condensation region, $2 < x/b \leq 3$, is also illustrated in Fig. 3. At early stages of the

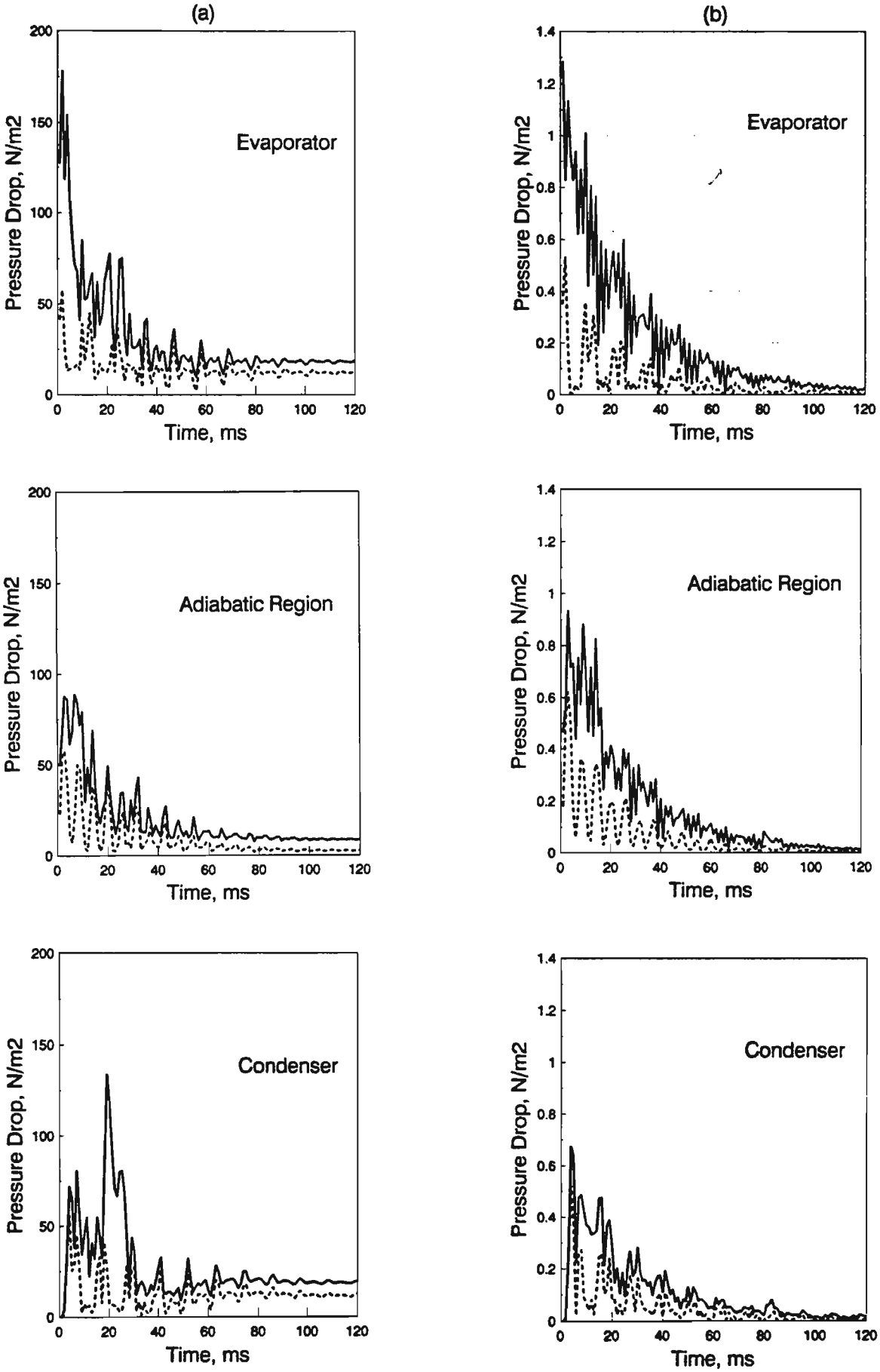

Fig. 6 Calculated pressure drops for (*a*) high- and (*b*) low-input heat fluxes (— and ··· denote maximum and maximum averaged pressure drops, respectively)

start-up transient process, the vapor is at the same temperature as the liquid and, therefore, there is no condensation (Figs. 3*a* and 3*b*). When vapor at the higher temperature flows from the evaporation to the condensation region, the vapor temperature on the condenser increases. A temperature gradient is then established along the liquid layer since the temperature at the outer surface of the liquid layer is kept fixed, and condensation takes place (Fig. 3*c*). The vapor temperature in the condenser increases with time and, consequently, the condensation rate increases. At steady state, shown in Fig. 3*i*, the mass flow through the evaporator equals the mass flow out of the condenser.

4.2 High-Input Heat Flux. The transient flow patterns for a relatively high heat flux, $\dot{q}_o'' = 10^6$ W/m^2, are shown in Fig. 4. The corresponding Reynolds number in this case is Re = 1000 and the optimized grid in this case in 41 × 121. The transient development of the vertical flow ρv at different times is shown (Fig. 4). In the evaporator region, multiple wave reflection and refill of vapor is observed to be the same as that for the low-input heat flux discussed above. In this case, however, the reversed flow caused by the wave reflection develops with time and is sustained as the process reaches steady-state operation.

At high-input heat flux, the flow pattern in the adiabatic region, $1 < x/b \leq 2$, is significantly different from that for lower heat fluxes. Figure 4(*d*) shows that when the reflected wave reaches the lower boundary of the evaporator, circulation is initiated in the adiabatic region. This circulation ceases when the vapor flow refills the evaporator region (Fig. 4*e*). However, the second reflection will cause a stronger circulation in the adiabatic region, as shown in Fig. 4(*f*). Figures 4(*g*)–4(*l*) demonstrate the subsequent sets of reflection and refill of the vapor flow with circulation strength increasing with time. When the procress reaches steady-state conditions, circulation occupies a significant portion of the region. Circulation in the adiabatic region was also found and reported by Issacci et al. (1989) in an analysis of the operational transient mode of heat pipes.

In order to show the overall picture of flow pattern development, Fig. 5 was prepared to depict the vapor flow fields at different times. Figure 5(*a*) shows the flow field at an early stage of the transient process after the first wave reflection. Here the wave reflection in the left top corner of the evaporation region is shown. The wave reflection initiates flow circulation at the entrance to the adiabatic region shown in Fig. 5(*b*). Vortex formation in the adiabatic region develops with time to a stronger flow circulation (Fig. 5*c*) and another vortex can be seen in the left corner of the evaporation region. In the flow field at steady state (Fig. 5*d*), it is seen that flow circulation in the adiabatic region develops to two vortices.

4.3 Pressure and Pressure Drop. One of the major issues in designing a heat pipe is to calculate correctly the pressure drop along the vapor core in different sections of the pipe. The correlations widely used in these calculations are based on a simple 1D steady-state analysis. In this section, the pressure drops in different sections of the heat pipe are shown as functions of time. The calculated pressure drops for high- and low-input ($\dot{q}_o'' = 10^6$ W/m^2 and 10^4 W/m^2, respectively) heat fluxes are shown in Fig. 6 for different times during the transient phase. Solid lines show the maximum pressure drop in a specific region of the pipe. Averaging the pressure along the vertical cross section of the pipe and then calculating the maximum-averaged pressure drop yields interesting results, which are shown by dotted lines for different times in different sections. Both the maximum and the maximum-averaged pressure drops display nearly periodic oscillation until they converge to a constant value at steady state. Pressure oscillations are caused by multiple wave reflections in the evaporation region (Figs. 3 and 4) and at each wave reflection, the local pressure increases significantly. Consequently, a large pressure difference is created along the pipe. The same type of oscillation in the vapor pressure, caused by reflection of compression waves, was also reported by Bowman and Hitchcock (1988).

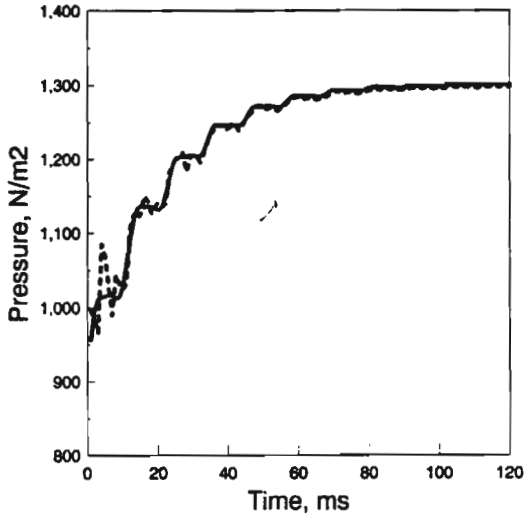

Fig. 7 Averaged (———) and saturated (···) vapor pressures in the evaporator

Another interesting result that can be seen in Fig. 6 is that the pressure drop is significantly higher during the initial period of the start-up transient of heat pipe operation. The mean value of the pressure drop decreases with time, and at steady state its value is less than 10 percent of the initial pressure drop. Therefore, if a heat pipe is designed to operate in the transient mode, the use of steady-state correlations may result in significant errors.

Tien and Rohani (1974) showed that the cross-sectional averaged pressure difference along a heat pipe is greater than the pressure difference calculated by Bankston and Smith (1973) using a 1D analysis. Here we compare the cross-sectional averaged pressure with the calculated 2D pressure by comparing the maximum pressure drops in both cases. Although the maximum-averaged pressure drops (dotted lines on Fig. 6) converge to the maximum pressure drops as the process approaches steady state, it is significantly lower during the initial transient time. This emphasizes the need for a 2D vapor flow model in an overall heat pipe transient analysis.

The pressure drop along the pipe, as mentioned before, plays an important role in the design of a heat pipe. In addition, the pressure in the evaporator may cause limitations on heat pipe operations. When a wave reflects in the evaporation region and the local pressure increases, the increase in the overall pressure of the evaporator may affect the evaporation rate. In order to study this aspect, the averaged (solid lines) and the saturated vapor pressures (dotted lines) in the liquid–vapor interface in the evaporator are shown as functions of time in Fig. 7. Here again, the periodic behavior of pressure is evident. During early transient times, the averaged pressure in the evaporator is sometimes larger than the saturated pressure. This will affect the evaporation process by decreasing the evaporation rate. Furthermore, whenever the vapor pressure is greater than the saturated pressure, condensation takes place by nucleation of mists in the vapor. In this case the flow is not homogeneous and a two-phase flow analysis should be incorporated. We have not done so.

4.4 Friction Factor. In order to design a heat pipe, it is necessary to calculate the friction factor coefficients of liquid on the vapor core. The averaged friction factor at the liquid–vapor interface along the pipe is calculated by

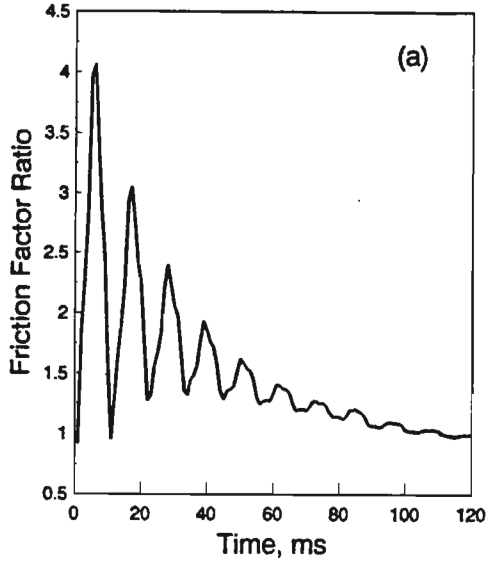

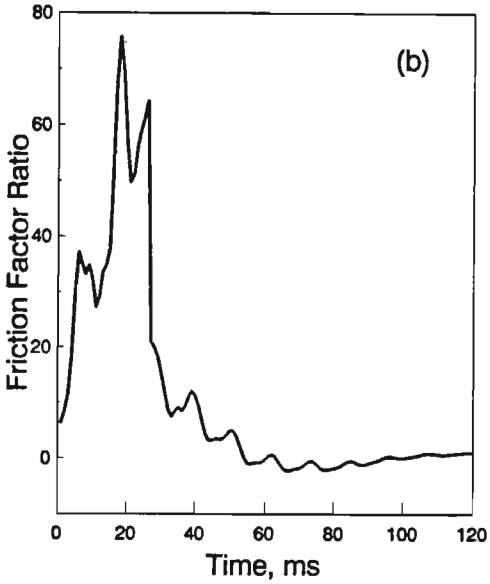

Fig. 8 Friction factors for (*a*) low- and (*b*) high-input heat fluxes

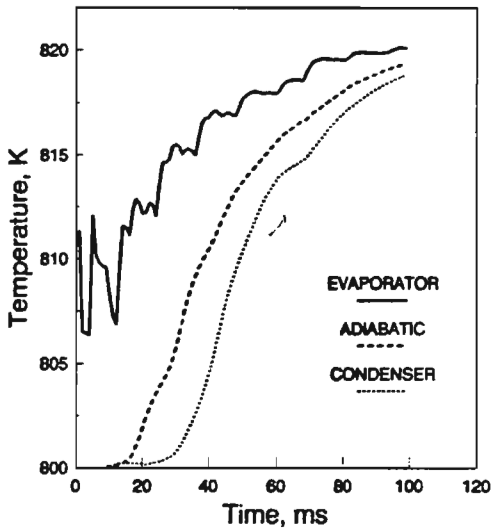

Fig. 9 Averaged vapor temperature

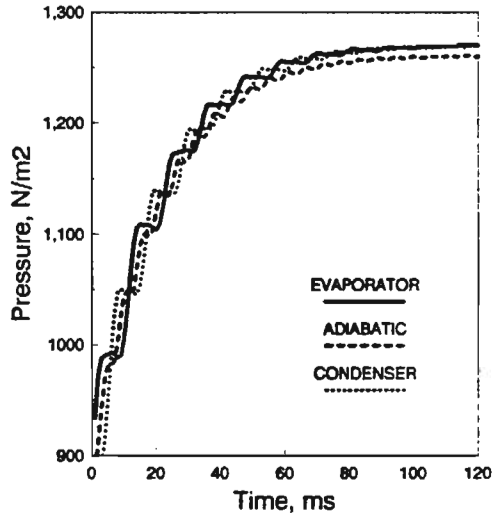

Fig. 10 Averaged vapor pressure

$$C_f(t) = \frac{\frac{1}{L}\int_0^L \tau_w dx}{\frac{1}{2}\rho u^2} = \frac{\frac{1}{L}\int_0^L \mu \left.\frac{du}{dy}\right|_{y=0} dx}{\frac{1}{2}\rho u^2} \tag{13}$$

The ratio of the averaged friction factor and its value at steady state, $C_f(t)/C_f(\infty)$, for low- and high-input heat fluxes are shown in Figs. 8(*a*) and 8(*b*), respectively. The friction factor oscillates periodically because of the wave reflections, and converges to a constant value at steady state. Figure 8(*a*) shows that for low-input heat flux ($\dot{q}_o'' = 10^4$ W/m^2), the maximum friction factor during the transient phase is about 50 percent more than its value at steady state. Note that during the times the friction factor is high, the wick could dry out. For high-input heat flux ($\dot{q}_o'' = 10^6$ W/m^2), the friction factor is about 35 times more than its steady-state value (Fig. 8*b*). This implies that in designing a heat pipe for transient operations, the steady-state correlations may cause a significant error.

4.5 Temperature, Pressure, and Axial Mass Flux. The variations of the averaged vapor temperature and pressure of the pipe are shown in Figs. 9 and 10, respectively. At an early stage of operation the temperature difference between the evaporator and the condenser is about 12 K, whereas at steady state, the temperature difference decreases to about 2 K. The effects of multiple reflections of the compression waves in the evaporator are also observed in these figures.

The development of the axial mass flux of the vapor flow with time is shown in Fig. 11 for the middle of the evaporator, $x = 0.5$, and for the middle of the pipe, $x = 1.5$. The vapor axial mass flux in the evaporator, Fig. 11(*a*), develops to a parabolic profile. However, in the adiabatic region, Fig. 11(*b*), a reverse flow is shown to grow with time.

5. Summary and Conclusions

A nonlinear filtering technique has been used to analyze the start-up vapor dynamics in heat pipes. Large variations in vapor compressibility during the transient phase render it inappropriate to use the SIMPLER scheme or to use standard schemes for the advective terms.

For a high heat flux, the start-up transient phase involves multiple wave reflections from the line of symmetry in the evaporator region. Each wave reflection causes a significant increase in the local pressure and a large pressure drop along the heat pipe. Furthermore, wave reflections cause flow reversal in the evaporation region and flow circulations in the adiabatic region. The vapor vortex formation in the evaporator is only transient and is observed to disappear as steady state

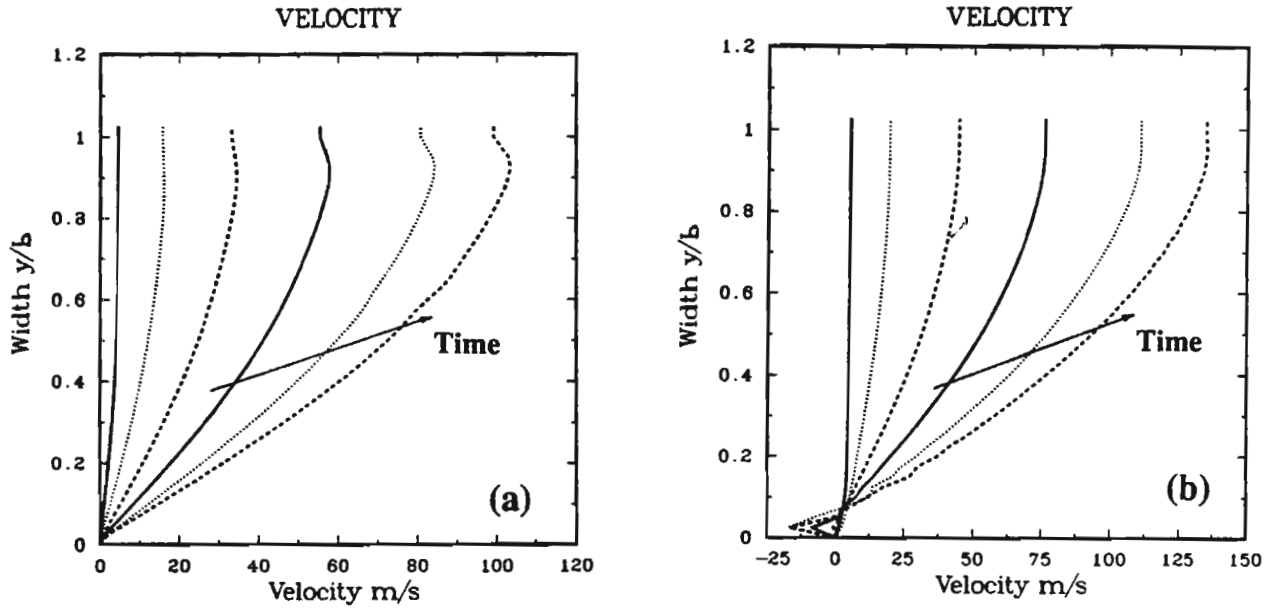

Fig. 11 Axial mass flux; (*a*) evaporator, (*b*) adiabatic region

is approached. However the circulation in the adiabatic region grows with time, and in the steady-state condition the circulation occupies a significant portion of the region.

The maximum and maximum-averaged pressure drops in different sections of the heat pipe oscillate periodically with time because of the multiple wave reflections in the evaporator. The pressure drops converge to a constant value at steady state. However, they are significantly higher than their steady-state value at the initiation of the start-up transient.

The pressure increase due to wave reflection may cause the overall pressure of the evaporator to be greater than the saturated vapor pressure. When this occurs, condensation takes place by mist nucleation in the vapor. Therefore, the condensation rate is expected to decrease.

The time for the vapor core to reach a steady-state condition depends on the input heat flux, the heat pipe geometry, the working fluid, and the condenser conditions. However, the vapor transient time is of the order of seconds. Depending on the time constant for the overall system, the vapor transient time may be very short. Therefore, the vapor core may be assumed quasi-steady in transient analysis of a heat pipe operation.

Acknowledgments

This work was supported by NASA-Lewis under Contract No. NAG3-899 and NASA Dryden under Contract No. NCC2-374 Supp. 2, and by the U.S. Department of Energy, Office of Fusion Energy, Grant No. DE-FG03-86ER52126, with UCLA.

References

Bankston, C. A., and Smith, H. J., 1973, "Vapor Flow in Cylindrical Heat Pipes," ASME JOURNAL OF HEAT TRANSFER, Vol. 95, pp. 371–376.

Bystrov, P. I., and Goncharov, V. F., 1983, "Starting Dynamics of High Temperature Gas-Filled Heat Pipes," *High Temperature*, Vol. 21, pp. 927–936.

Bowman, W. J., 1987, "Simulated Heat Pipe Vapor Dynamics," Ph.D. Dissertation, Air Force Institute of Technology.

Bowman, W. J., and Hitchcock, J. E., 1988, "Transient, Compressible Heat-Pipe Vapor Dynamics," *Proceedings, 24th National Heat Transfer Conderence*, Vol. 1, pp. 329–337, Houston, TX.

Bowman, W. J., McClure, W. C., and Towne, M., 1990, "Transient Heat-Pipe Modeling, Paper 2," AIAA Paper No. 90-0061.

Chakravarthy, S., and Osher S., 1982, "Numerical Experiments With the Osher Upwind Scheme for the Euler Equations," *Proceedings, Joint Fluids, Plasma, Thermophysics and Heat Transfer Conference*, AIAA/ASME, St. Louis, MO.

Chow, L., and Zhong, J., 1990, "Analysis of Heat Pipe Start-Up From the Frozen State," presented at the AIAA/ASME 5th Joint Thermophysics and Heat Transfer Conference, Seattle, WA.

Edwards, D. K., and Marcus, B. D., 1972, "Heat and Mass Transfer in the Vicinity of the Vapor–Gas Front in a Gas-Loaded Heat Pipe," ASME JOURNAL OF HEAT TRANSFER, Vol. 94, No. 2, pp. 155–162.

Engquist, B., Lötstedt, P., and Sjögreen, B., 1989, "Nonlinear Filters for Efficient Shock Computation," *J. Math. Comp.*, Vol. 52, No. 186, pp. 509–537.

Faghri, A., 1986, "Vapor Flow Analysis in a Double-Walled Concentric Heat Pipe," *Numerical Heat Transfer*, Vol. 10, pp. 583–596.

Faghri, A., Chen, M-M., and Mahefkey, E. T., 1989, "Simultaneous Axial Conduction in the Fluid and the Pipe Wall for Forced Convective Laminar Flow With Blowing and Suction at the Wall," *Int. J. Heat Mass Transfer*, Vol. 32, No. 2, pp. 281–288.

Hall, M. L., and Doster, J. M., 1988, "The THROUPUT Code: Thermo-hydraulic Heat Pipe Modeling," *Proceedings, 5th Symposium on Space Nuclear Power Systems*, Institute for Space Nuclear Power Studies, University of New Mexico.

Hall, M. L., and Doster, J. M., 1990, "A Sensitivity Study of the Effects of Evaporation/Condensation Accommodation Coefficients on Transient Heat Pipe Modeling," *Int. J. Heat Mass Transfer*, Vol. 33, No. 3, pp. 465–481.

Harten, A., and Zwas, G., 1972, "Switched Numerical Shuman Filters for Shock Calculations," *J. Engrg. Math.*, Vol. 6, pp. 207–216.

Harten, A., 1983, "High Resolution Schemes for Hyperbolic Conservation Laws," *J. Comp. Phys.*, Vol. 49, pp. 357–393.

Issacci, F., Roche, G. L., Klein, D. B., and Catton, I., 1988, "Heat Pipe Vapor Dynamics," University of California—Los Angeles, Report No. UCLA-ENG-88-28.

Issacci, F., Catton, I., Heiss, A., and Ghoniem, N. M., 1989, "Analysis of Heat Pipe Vapor Flow Dynamics," *Chem. Eng. Comm.*, Vol. 85, pp. 85–94.

Issacci, F., Catton, I., and Ghoniem, N. M., 1990a, "Vapor Dynamics of Heat Pipe Start-Up," *Proceedings, 7th Symposium on Space Nuclear Power Systems*, Vol. 2, pp. 1002–1007, Institute for Space Nuclear Power Studies, University of New Mexico.

Issacci, F., McDonough, J. M., Catton, I., and Ghoniem, N. M., 1990b, "Nonlinear Filtering for Shock Capturing and Cell-Reynolds Number Problems in Compressible Vapor Dynamics," submitted to *J. Comp. Phys.*

Jang, J. H., Faghri, A., Chang, W. S., and Mahefkey, E. T., 1989, "Mathematical Modeling and Analysis of Heat Pipe Startup From the Frozen State," in: *Heat Transfer With Phase Change*, ASME HTD-Vol. 114.

Patankar, S. V., 1980, *Numerical Heat Transfer and Fluid Mechanics*, McGraw-Hill, New York.

Peterson, P. F., and Tien, C. L., 1987, "Gas-Concentration Measurements and Analysis for Gas-Loaded Thermosyphons," *Proceedings, International Symposium on Natural Circulation*, ASME HTD, Boston, MA.

Rao, D. V., El-Genk, M. S., and Juhasz, A. J., 1990, "Transient Model of High Temperature Heat Pipes," *Proceedings, 7th Symposium on Space Nuclear Power Systems*, Institute for Space Nuclear Power Studies, University of New Mexico.

Roche, G. L., 1988, "Analytical Studies of the Liquid Phase Transient Behavior of a High Temperature Heat Pipe," M. S. Thesis, University of California—Los Angeles.

Runchal, A. K., 1987, "CONDIF: A Modified Central-Difference Scheme for Convective Flows," *Int. J. Numer. Methods Eng.*, Vol. 24, No. 8, pp. 1593–1608.

Tien, C. L., and Rohani, A. R., 1974, "Analysis of the Effects of Vapor Pressure Drop on Heat Pipe Performance," *Int. J. Heat Mass Transfer*, Vol,. 17, pp. 61–67.